Heliyon 9 (2023) e18056

Contents lists available at ScienceDirect

Heliyon

journal homepage: www.cell.com/heliyon

Novel clinical radiomic nomogram method for differentiating malignant from non-malignant pleural effusions

Rui Han [a,1], Ling Huang [b,1], Sijing Zhou [c,1], Jiran Shen [a], Pulin Li [a], Min Li [d], Xingwang Wu [e,**], Ran Wang [a,*]

[a] Department of Respiratory and Critical Care Medicine, The First Affiliated Hospital of Anhui Medical University, Hefei, 230022, China
[b] Department of Infectious Disease, Hefei Second People's Hospital, Hefei, 230001, China
[c] Department of Occupational Disease, Hefei Third Clinical College of Anhui Medical University, Hefei, 230022, China
[d] Department of Oncology, The First Affiliated Hospital of Anhui Medical University, Hefei, 230022, China
[e] Department of Radiology, The First Affiliated Hospital of Anhui Medical University, Hefei, 230022, China

ARTICLE INFO

Keywords:
Pleural effusion
Computed tomography
Radiomics
Nomogram

ABSTRACT

Objectives: To establish a clinical radiomics nomogram that differentiates malignant and non-malignant pleural effusions.
Methods: A total of 146 patients with malignant pleural effusion (MPE) and 93 patients with non-MPE (NMPE) were included. The ROI image features of chest lesions were extracted using CT. Univariate analysis was performed, and least absolute shrinkage selection operator and multivariate logistic analysis were used to screen radiomics features and calculate the radiomics score. A nomogram was constructed by combining clinical factors with radiomics scores. ROC curve and decision curve analysis (DCA) were used to evaluate the prediction effect.
Results: After screening, 19 radiomics features and 2 clinical factors were selected as optimal predictors to establish a combined model and construct a nomogram. The AUC of the combined model was 0.968 (95% confidence interval [CI] = 0.944–0.986) in the training cohort and 0.873 (95% CI = 0.796–0.940) in the validation cohort. The AUC value of the combined model was significantly higher than those of the clinical and radiomics models (0.968 vs. 0.874 vs. 0.878, respectively). This was similar in the validation cohort (0.873, 0.764, and 0.808, respectively). DCA confirmed the clinical utility of the radiomics nomogram.
Conclusion: CT-based radiomics showed better diagnostic accuracy and model fit than clinical and radiological features in distinguishing MPE from NMPE. The combination of both achieved better diagnostic performance. These findings support the clinical application of the nomogram in diagnosing MPE using chest CT.

1. Introduction

Pleural effusion is an excess of fluid in the pleural cavity that is usually due to an imbalance in the rate of normal pleural effusion production and/or absorption [1]. Pleural effusion is associated with a range of potential causes, including physical trauma or systemic

* Corresponding author.
** Corresponding author.
E-mail addresses: wuxingwangahmu@163.com (X. Wu), wangran@ahmu.edu.cn (R. Wang).
[1] These authors contributed equally to this work.

https://doi.org/10.1016/j.heliyon.2023.e18056
Received 19 December 2022; Received in revised form 29 June 2023; Accepted 5 July 2023
Available online 13 July 2023

Abbreviations and acronyms

LDH	lactate dehydrogenase
DCA	decision curve analysis
OR	odds ratio
CI	confidence interval
VIF	variance inflation factor
ICCs	inter- and intra-class correlation coefficients
SLDHPADA	serum lactate dehydrogenase/pleural effusion adenosine deaminase
PCEA1	pleural effusion/serum carcinoembryonic antigen
NMPE	non-MPE
MPE	malignant pleural effusion

diseases (such as inflammation, infection, or cancer) [2]. When evaluating patients with pleural effusion, the first step is to distinguish between inflammatory (exudative) and noninflammatory (transudative) effusions [3]. If an exudative effusion is present, further diagnostic procedures such as cytopathology, pleural biopsy, and sometimes even thoracotomy must be performed to make a definite diagnosis and to allow specific treatment of pleural disease [4]. Light's criteria have been used to distinguish exudative and transudative effusions since 1972 [4]. Accordingly, exudative effusion is diagnosed if any of the following conditions are met: total protein level >3 g/100 mL or pleural fluid/serum total protein ratio >0.5, pleural fluid/serum lactate dehydrogenase (LDH) ratio >0.6, and pleural fluid LDH greater than two-thirds of the upper limit of normal serum LDH levels [4–7].

Malignant effusions are exudates that meet at least one of these criteria, and malignant disease is one of the main causes of pleural effusions [7]. More than 90% of malignant effusions are due to metastasis, usually from primary tumors in the lung or breast [7–9]. In clinical practice, the focus is on differentiating malignant pleural effusion (MPE) from non-malignant pleural effusion (NMPE). Cytological analysis of pleural effusion is the simplest and definitive method for diagnosing MPE. However, the sensitivity of cytological analysis is between 40% and 70% because malignant cells may be absent, overlooked, or incorrectly identified in the sample [10–12].

Chest computed tomography (CT) scan with contrast media is an important means to detect pleural effusion. If pleural effusion has complex ultrasonographic features, such as septation and localization, that may suggest parapulmonary effusions or malignancy, CT is generally recommended [13]. CT scans of the chest can provide clues to potential pathology (e.g., pulmonary infiltration, mass or embolism, mediastinal lymph-node involvement, or pericardial involvement) in patients with pleural effusion [14]. Radiomics

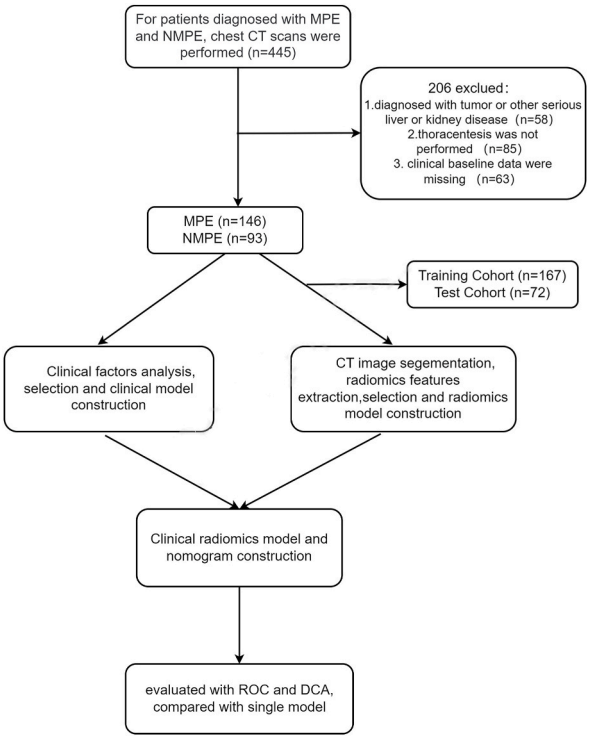

Fig. 1. The flow diagram of study.

involves the extraction of high-throughput quantitative features from digitized radiological images [15]. These features can be applied in clinical decision support systems or to develop meaningful imaging biomarkers for classifying pathological subtypes and predicting specific genomic patterns, clinical outcomes, treatment response, and survival in various diseases to improve diagnostic, prognostic, and predictive accuracy [16]. Radiomics have been widely used in the oncology [17–19]. However, to our knowledge, radiomics has not been used to differentiate MPE and NMPE.

In this study, we developed a clinical radiomics nomogram to distinguish MPE from NMPE for improved diagnosis and timely treatment.

2. Materials and methods

2.1. Patients

The personal information of the patients included in the study was strictly protected. During data collection, the identity of the patients is anonymized, so we only number them, and we do not expose the personal information of the patients in the paper. Because of the retrospective nature of this study, patients' identities were anonymized, and therefore informed consent was waived, which is a feature of observational studies and has been done in several previous articles. However, an ethics approval number was obtained from the study institution. The inclusion criteria were as follows: (1) patients who underwent low-dose CT scan; (2) the CT images were of sufficient quality for interpretation; (3) the malignant tissue in the pleural space had been visualized by pleural biopsy, cytopathology, or autopsy for the diagnosis of malignant effusions [4,7]; and (4) clinical data, including age, sex, and smoking history, were available. The exclusion criteria were as follows: (1) other serious liver or kidney diseases, (2) thoracentesis not performed, and (3) missing clinical baseline data.

A total of 239 patients (146 with MPE and 93 with NMPE) were enrolled in the study. Our MPE patients included not only patients with lung cancer, but also patients with other cancers, such as gastrointestinal tumors, breast malignancies, and liver malignancies. Among them, lung cancer accounted for 73.97%. All patients were treated after CT scanning. The time interval between treatment and CT scanning was within two weeks. The flow diagram of the study is shown in Fig. 1. Baseline clinical data included age, sex, smoking history, body mass index, pleural effusion cytology, and pleural effusion albumin, pleural effusion LDH, pleural effusion pondus hydrogenii, pleural effusion/serum carcinoembryonic antigen (PCEA1), serum lactate dehydrogenase/pleural effusion adenosine deaminase (SLDHPADA), white blood cell, red blood cell, hemoglobin, platelet, and neutrophil, Lymphocyte, neutrophil/lymphocyte, platelet/lymphocyte, neutrophil/lymphocyte $\times$ platelet, and *C*-reactive protein levels.

2.2. CT protocol

All patients underwent chest unenhanced low-dose CT scans on a 64-row Discover CT750HD (GE Healthcare) scanner. The coverage area extended from the entrance of the thoracic cavity to the diaphragm. Following the institutional guidelines for low-dose CT scanning, all chest CT studies were performed with specified parameters (5 mm slice thickness, 100 kVp tube voltage, automatic tube current modulation technique, and 1.375 helical pitch) to achieve an image noise index of 1113 HU. The CT dose index volume was 1.67 $\pm$ 0.83 mGy, and the dose length product was 41.54 $\pm$ 22.78 mGy $\times$ cm.

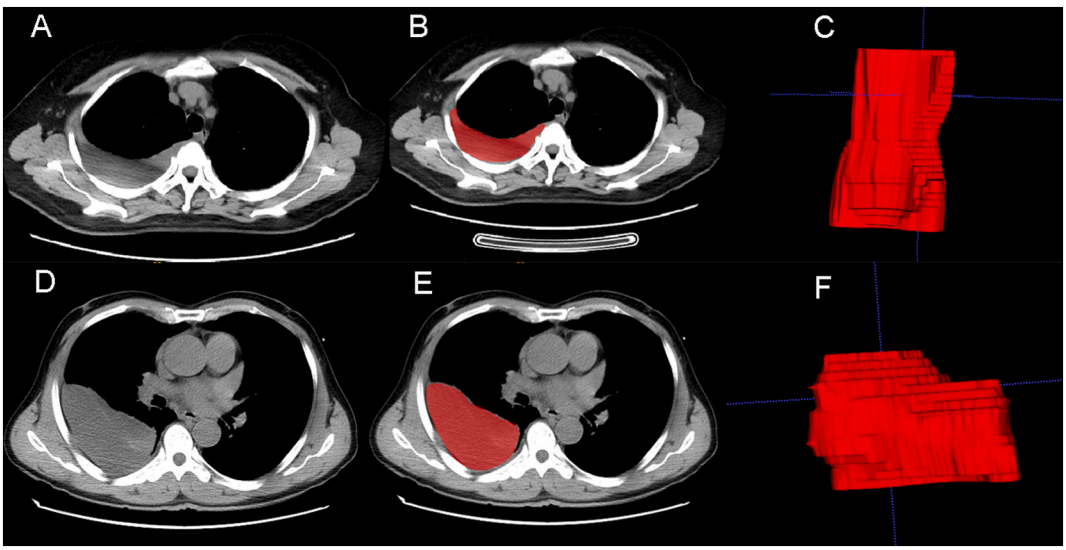

Fig. 2. ROI segmentation. (A and D) Original CT image of a patient with pleural effusion. (B and E) Layer-by-layer delineation of pleural effusion lesions on CT images. (C and F) 3D ROI of pleural effusion lesions.

2.3. Radiomics workflow and imaging analyses, segmentation, and feature extraction

The radiomics workflow used in this study is divided into the following parts: image acquisition, region of interest (ROI) segmentation, radiomics feature extraction, feature selection, model construction in the training cohort, and performance evaluation of the radiomics model.

For each patient, the ROI was acquired using ITK-SNAP 3.8.0 (ITK-SNAP Home (itksnap.org)) by a radiologist (10 years of experience in CT imaging) and then confirmed by another radiologist (>20 years of experience in CT imaging). If there were different interpretations, a final consensus was reached through group discussion.

All images were sketched at the same window width and level (window width 300 HU, window level 30 HU). We imported dicom files into ITK-SNAP for ROI delineation. To ensure consistency in lesion ROI selection and to avoid bias, we selected the region containing the pleural effusion, including the top, bottom, and largest levels of pleural effusion, and then we connected each level (Fig. 2). As shown in Fig. 2A and D are the original CT image of pleural effusion, and Fig. 2B and E are the maximum plane of pleural effusion selected by us. We successively depicted the top contour, the maximum horizontal plane contour, the bottom contour and the several contours between the top and the bottom on each CT image, and finally connected each contour to form 3D ROI (Fig. 2C and F). The 3D active contour segmentation is implemented [20], and the right side is the 3D model obtained by our final connection. If the patient presented with bilateral pleural effusions, our image delineation was performed simultaneously on both sides to include all areas as much as possible. We used inter- and intra-class correlation coefficients (ICCs) to evaluate the consistency and reproducibility of the results. We randomly selected images from 50 patients. A total of 239 subjects were randomly divided into groups directly, and random numbers were generated by random number table for randomization, and no restrictions, intervention or adjustment were made during the implementation. ROI selection was performed by readers 1 and 2. After two weeks, the same procedure was repeated by reader 1. A higher ICC value indicates higher repeatability and vice versa. Based on the 95% confidence interval of the ICC estimate, values of less than 0.5, between 0.5 and 0.75, between 0.75 and 0.9, and greater than 0.90 indicated poor, moderate, good, and excellent reliability, respectively [21]. Therefore, features with ICCs≤0.75 were considered to be less consistent with features, and so they were removed. When the ICCs were >0.75, feature extraction had a good consistency. ROI selection of the remaining images was performed by reader 1.

Table 1
Baseline characteristics of all patients.

Characteristics	MPE (n = 146)	NMPE (n = 93)	P value
Gender, n (%)			0.436
Female	54 (22.6%)	29 (12.1%)	
Male	92 (38.5%)	64 (26.8%)	
Smoking, n (%)			0.783
No	62 (25.9%)	37 (15.5%)	
Yes	84 (35.1%)	56 (23.4%)	
Cytology, n (%)			<0.001
No*	102 (42.7%)	93 (38.9%)	
Yes*	44 (18.4%)	0 (0%)	
PLDH1, n (%)			0.762
No	78 (32.6%)	47 (19.7%)	
Yes	68 (28.5%)	46 (19.2%)	
PCEA1, n (%)			<0.001
No	50 (20.9%)	65 (27.2%)	
Yes	96 (40.2%)	28 (11.7%)	
SLDHPADA, n (%)			<0.001
No	22 (9.2%)	64 (26.8%)	
Yes	124 (51.9%)	29 (12.1%)	
Age, median (IQR)	68 (57.25, 74)	57 (42, 68)	<0.001
BMI, median (IQR)	22.15 (19.75, 23.88)	20.96 (19.72, 22.86)	0.066
PALB, median (IQR)	40.5 (33.2, 47.2)	44.5 (24.6, 49.5)	0.808
PLDH, median (IQR)	443 (245.5, 989)	468 (205, 1180)	0.908
pH, median (IQR)	7.1 (7, 7.2)	7.1 (6.8, 7.2)	0.849
WBC, median (IQR)	6.88 (5.34, 9.02)	6.12 (4.53, 7.82)	0.026
RBC, median (IQR)	3.91 (3.47, 4.44)	4 (3.39, 4.32)	0.441
HGB, median (IQR)	117.5 (101, 132)	118 (96, 130)	0.415
PLT, median (IQR)	244.5 (178.5, 319)	233 (164, 339)	0.845
N, median (IQR)	4.88 (3.41, 6.8)	4.4 (3.23, 5.36)	0.026
L, median (IQR)	1.12 (0.84, 1.53)	1.01 (0.72, 1.44)	0.272
NLR, median (IQR)	4.27 (2.49, 7.31)	4 (2.68, 6.56)	0.581
PLR, median (IQR)	205.05 (147.96, 301.23)	232.61 (158.02, 302.56)	0.331
SII, median (IQR)	988.87 (539.81, 1805.87)	1035.45 (586.27, 1592.22)	0.885

Abbreviations: No*, No cancer cells were detected; Yes*, Detection of cancer cells; PLDH1, The lactate dehydrogenase level of pleural effusion was >500 U/L; PCEA1, Pleural effusion/serum carcino-embryonic antigen > 1; SLDHPADA, Serum lactate dehydrogenase/pleural effusion adenosine deaminase > 20; BMI, Body mass index; IQR, Interquartile range; pH, Pondus hydrogenii; WBC, Blood white blood cell; RBC, Red blood cell; HGB, Hemoglobin; PLT, Platelet; N, Neutrophil; L, Lymphocyte; NLR, Neutrophil/lymphocyte; PLR, Platelet/lymphocyte; SII, Neutrophil/lymphocyte × platelet.

In order to eliminate the influence of different sources of data on the results, image normalization has been a standard procedure for radiomics. All images were resampled (voxel size 1 × 1 × 1 mm) and normalized before extracting radiomics features. Z-score was used to normalize the image data to achieve zero mean and unit variance in the training and validation cohorts, with the following format: $z = (x - \mu)/\sigma$ (x: sample value; μ: population mean; σ: population standard deviation). Radiomics features were extracted using PyRadiomics, an open-source radiomics toolkit [22]. Radiomics feature sets can be divided into several families, including statistical, intensity histogram-based, intensity-volume histogram-based, morphological, local intensity, and texture features [23]. The Imaging Biomarker Standardization Initiative (IBSI) is an independent international collaborative organization dedicated to the standardization of imaging biomarkers, and our radiomics is IBSI compliant [23]. A total of 1687 quantitative radiomics features were extracted from the CT images of each patient.

3. Model development and classification

3.1. Clinical model

The clinical baseline data for MPE and NMPE are shown in Table 1. Univariate analysis was performed to identify clinical features with $p < 0.05$ between MPE and NMPE. Multivariate logistic regression analysis was performed to evaluate multicollinearity using the variance inflation factor (VIF), and factors with VIF >10 were excluded from the regression model. Finally, $p < 0.01$ was considered as an independent predictor, and the prediction model of clinical factors was established.

3.2. Radiomics model

IPMs 2.4.0 (GE Healthcare) software was used for data preprocessing and feature selection. The datasets were randomly assigned to either the training or test cohorts in a ratio of 7:3. All cases in the training cohort were used to train the prediction model. All cases in the test cohort were used to independently evaluate the model performance. Variables with zero variance were eliminated before the analysis, and missing values were filled in with medians. The data were standardized and processed with the Z-score.

First, the ICCs >0.75 feature was preserved. Second, features with $p < 0.05$ were selected using univariate logistic analysis. Third, multivariate logistic analysis was used to further identify the most useful features, and a stepwise selection method was used for feature selection. Fourth, the independent risk predictors were retained ($p < 0.05$). Finally, a logistic-based rad-score model was built on the basis of the established optimal feature subsets of the training dataset.

In addition, we constructed a combined model by integrating two selected clinical factors and radiomics features from the clinical model. Five-fold cross-validation was performed in all radiomics signature-building procedures. The radiomics signature was tested in an independent validation cohort, and its discrimination performance was evaluated using ROC curve analysis and quantified using the AUC [24].

Finally, the two selected clinical factors were combined with the radiomics score to construct a clinical radiomics nomogram using a multivariate logistic regression analysis.

3.3. Statistical analyses

ROC curves were generated to evaluate the performance of the machine learning model. Accuracy, sensitivity, specificity, and AUC were calculated. All statistical analyses in this study were performed using R 4.1.2 (R: The R Project for Statistical Computing (r-project.org)) and SPSS 26.0 (SPSS Software, IBM). Differences between patient groups (responders and non-responders) in characteristic variables and clinical parameters were assessed using the Mann–Whitney *U* test for continuous variables and the chi-square test for categorical variables. A two-tailed *p*-value of less than 0.05 was considered statistically significant. Decision curve analysis (DCA), a statistical method used to assess whether a model has utility to support clinical decision making, can be used to determine which of the two models leads to the best decision. Therefore, it is an essential validation tool on top of measures such as identification and calibration.

4. Results

4.1. Establishment of the clinical model

According to the inclusion and exclusion criteria, 239 eligible patients with MPE and NMPE were included in this study, including 146 with MPE and 93 with NMPE. All baseline characteristics of the patients are shown in Table 1. In the training cohort, two independent predictors were screened using univariate and multivariate logistic regression analyses, and the differences between MPE and NMPE were statistically significant ($p < 0.01$): PCEA1 (odds ratio (OR) = 0.226, 95% confidence interval (CI) = 0.083–0.614, $p = 0.004$) and SLDHPADA (OR = 0.122, 95% CI = 0.043–0.349, $p < 0.001$). We further present the clinical characteristics of MPE/NMPE in the training and validation cohorts in Tables 1a and 1b, respectively.

4.2. Establishment of the radiomics model

A total of 1687 features were obtained from each ROI. The top 19 radiomics features are listed in Table 2.

The rad-score for each patient was calculated using the following formula:

$$Rad-score = 0.8299 + 0.1365 \times original\_firstorder\_Kurtosis+$$

$$0.2048 \times original\_glszm\_LargeAreaLowGrayLevelEmphasis+$$

$$0.2602 \times wavelet\_LLH\_glcm\_Correlation-$$

$$0.3582 \times wavelet\_LHL\_firstorder\_Kurtosis-$$

$$0.4819 \times wavelet\_LHH\_firstorder\_Kurtosis-$$

$$0.2312 \times wavelet\_HLL\_glcm\_MCC+$$

$$0.7749 \times wavelet\_HHH\_glcm\_Imc1+$$

$$0.2251 \times square\_glszm\_SizeZoneNonUniformityNormalized-$$

$$0.5247 \times squareroot\_firstorder\_Kurtosis+$$

$$0.5890 \times squareroot\_gldm\_LargeDependenceLowGrayLevelEmphasis+$$

$$0.0969 \times exponential\_glcm\_Imc1-$$

$$0.3188 \times gradient\_gldm\_SmallDependenceLowGrayLevelEmphasis+$$

Table 1A
Baseline characteristics of training cohort.

Characteristics	MPE (n = 102)	NMPE (n = 44)	P value
Gender, n (%)			0.396
Female	62 (42.5%)	30 (20.5%)	
Male	40 (27.4%)	14 (9.6%)	
Smoking, n (%)			0.327
No	56 (38.4%)	28 (19.2%)	
Yes	46 (31.5%)	16 (11%)	
Cytology, n (%)			0.891
No*	73 (50.0%)	31 (21.2%)	
Yes*	29 (19.9%)	13 (8.9%)	
PLDH1, n (%)			0.103
No	43 (29.5%)	25 (17.1%)	
Yes	59 (40.4%)	19 (13%)	
PCEA1, n (%)			0.463
No	69 (47.3%)	27 (18.5%)	
Yes	33 (22.6%)	17 (11.6%)	
SLDHPADA, n (%)			0.089
No	90 (61.6%)	34 (23.3%)	
Yes	12 (8.2%)	10 (6.8%)	
Age, median (IQR)	67 (56.25, 73)	69 (59.75, 76.75)	0.167
BMI, median (IQR)	21.694 (19.648, 24.69)	22.584 (20.152, 23.677)	0.707
PALB, median (IQR)	40.8 (32, 47.5)	40.5 (35.95, 46.475)	0.700
PLDH, median (IQR)	397.5 (243, 985.75)	563.5 (297, 981)	0.492
PH, median (IQR)	7.1 (7, 7.2)	7 (6.95, 7.2)	0.468
WBC, median (IQR)	6.805 (5.2025, 9.015)	6.985 (5.545, 9.005)	0.981
RBC, mean ± sd	3.8715 ± 0.77401	3.9932 ± 0.62535	0.359
HGB, mean ± sd	114.75 ± 23.274	119.41 ± 19.017	0.208
PLT, median (IQR)	247.5 (180.25, 328.75)	231.5 (167, 305)	0.317
N, median (IQR)	4.88 (3.37, 6.7875)	4.88 (3.4825, 6.9075)	0.644
L, median (IQR)	1.16 (0.88, 1.5975)	0.985 (0.78, 1.3775)	0.071
NLR, median (IQR)	3.6194 (2.3398, 6.8066)	5.1104 (3.1063, 8.365)	0.093
PLR, median (IQR)	204.49 (143.03, 293.06)	218.12 (153.76, 312.35)	0.462
SII, median (IQR)	930.05 (519.17, 1741.1)	1034.1 (589.75, 2101.1)	0.459

Abbreviations: No*, No cancer cells were detected; Yes*, Detection of cancer cells; PLDH1, The lactate dehydrogenase level of pleural effusion was >500 U/L; PCEA1, Pleural effusion/serum carcino-embryonic antigen > 1; SLDHPADA, Serum lactate dehydrogenase/pleural effusion adenosine deaminase > 20; BMI, Body mass index; IQR, Interquartile range; pH, Pondus hydrogenii; WBC, Blood white blood cell; RBC, Red blood cell; HGB, Hemoglobin; PLT, Platelet; N, Neutrophil; L, Lymphocyte; NLR, Neutrophil/lymphocyte; PLR, Platelet/lymphocyte; SII, Neutrophil/lymphocyte × platelet.

Table 1B
Baseline characteristics of validation cohort.

Characteristics	MPE (n = 65)	MPE (n = 28)	P value
Gender, n (%)			0.536
Female	19 (20.4%)	10 (10.8%)	
Male	46 (49.5%)	18 (19.4%)	
Smoking, n (%)			0.390
No	24 (25.8%)	13 (14%)	
Yes	41 (44.1%)	15 (16.1%)	
Cytology, n (%)			0.874
No*	63 (67.7%)	28 (30.1%)	
Yes*	2 (2.2%)	0 (0%)	
PLDH1, n (%)			0.603
No	34 (36.6%)	13 (14%)	
Yes	31 (33.3%)	15 (16.1%)	
PCEA1, n (%)			0.439
No	47 (50.5%)	18 (19.4%)	
Yes	18 (19.4%)	10 (10.8%)	
SLDHPADA, n (%)			0.536
No	19 (20.4%)	10 (10.8%)	
Yes	46 (49.5%)	18 (19.4%)	
Age, median (IQR)	61 (43, 69)	52.5 (38.5, 63.25)	0.084
BMI, median (IQR)	21.05 (20.245, 22.647)	20.64 (18.409, 23.116)	0.212
PALB, median (IQR)	44.5 (28, 50.1)	44.55 (24.175, 48)	0.578
PLDH, median (IQR)	405 (253, 958)	627 (172.5, 1413.5)	0.782
PH, median (IQR)	7.1 (7, 7.2)	7.1 (6.8, 7.225)	0.645
WBC, median (IQR)	6.12 (4.36, 7.59)	6.22 (4.7125, 7.885)	0.477
RBC, median (IQR)	4.07 (3.39, 4.32)	3.925 (3.4175, 4.395)	0.927
HGB, median (IQR)	118 (96, 129)	116 (98.75, 130.5)	1.000
PLT, median (IQR)	214 (159, 339)	248.5 (186.5, 323.75)	0.377
N, median (IQR)	4.33 (3.05, 5.36)	4.73 (3.41, 5.355)	0.456
L, median (IQR)	0.97 (0.71, 1.31)	1.335 (0.795, 1.6675)	0.101
NLR, median (IQR)	4.027 (2.6765, 7.0615)	3.5382 (2.6973, 5.4911)	0.350
PLR, median (IQR)	233.63 (166.99, 291.55)	210.46 (155.05, 349.28)	0.760
SII, median (IQR)	1072.4 (643.66, 1675)	835.31 (498.58, 1255.7)	0.289

Abbreviations: No*, No cancer cells were detected; Yes*, Detection of cancer cells; PLDH1, The lactate dehydrogenase level of pleural effusion was >500 U/L; PCEA1, Pleural effusion/serum carcino-embryonic antigen > 1; SLDHPADA, Serum lactate dehydrogenase/pleural effusion adenosine deaminase > 20; BMI, Body mass index; IQR, Interquartile range; pH, Pondus hydrogenii; WBC, Blood white blood cell; RBC, Red blood cell; HGB, Hemoglobin; PLT, Platelet; N, Neutrophil; L, Lymphocyte; NLR, Neutrophil/lymphocyte; PLR, Platelet/lymphocyte; SII, Neutrophil/lymphocyte × platelet.

Table 2
Radiomic features selection from the CT in the training cohort.

Feature Selected	Group	Coef.
original_firstorder_Kurtosis	Firstorder	0.1365
original_glszm_LargeAreaLowGrayLevelEmphasis	GLSZM	0.2048
wavelet_LLH_glcm_Correlation	GLCM	0.2602
wavelet_LHL_firstorder_Kurtosis	Firstorder	−0.3582
wavelet_LHH_firstorder_Kurtosis	Firstorder	−0.4819
wavelet_HLL_glcm_MCC	GLCM	−0.2312
wavelet_HHH_glcm_Imc1	GLCM	0.7749
square_glszm_SizeZoneNonUniformityNormalized	GLSZM	0.2251
squareroot_firstorder_Kurtosis	Firstorder	−0.5247
squareroot_gldm_LargeDependenceLowGrayLevelEmphasis	GLDM	0.5890
exponential_glcm_Imc1	GLCM	0.0969
gradient_gldm_SmallDependenceLowGrayLevelEmphasis	GLDM	−0.3188
gradient_glszm_LargeAreaHighGrayLevelEmphasis	GLSZM	0.3103
lbp_3D_m2_glszm_GrayLevelNonUniformity	GLSZM	0.8623
lbp_3D_m2_glszm_ZoneVariance	GLSZM	0.3474
lbp_3D_k_firstorder_Skewness	Firstorder	0.1411
lbp_3D_k_glcm_ClusterShade	GLCM	0.3996
lbp_3D_k_glcm_MCC	GLCM	−0.1229
lbp_3D_k_glszm_LowGrayLevelZoneEmphasis	GLSZM	0.5653

$$0.3103 \times gradient\_glszm\_LargeAreaHighGrayLevelEmphasis+$$

$$0.8623 \times lbp\_3D\_m2\_glszm\_GrayLevelNonUniformity+$$

$$0.3474 \times lbp\_3D\_m2\_glszm\_ZoneVariance+$$

$$0.1411 \times lbp\_3D\_k\_firstorder\_Skewness+$$

$$0.3996 \times lbp\_3D\_k\_glcm\_ClusterShade-$$

$$0.1229 \times lbp\_3D\_k\_glcm\_MCC+$$

$$0.5653 \times lbp\_3D\_k\_glszm\_LowGrayLevelZoneEmphasis$$

In the training cohort, a significant difference was observed in the radiomics scores between the MPE and NMPE groups ($p < 0.05$). This was also true for the validation cohort ($p < 0.05$). The AUC and accuracy of the radiomics features were 0.878 (95% CI = 0.833–0.918) and 0.796 in the training cohort and 0.808 (95% CI = 0.713–0.894) and 0.722 in the validation cohort, respectively.

ROC curves were used to evaluate the performance of the established models (Table 3). The ROC curve showed that the clinical radiomics model (combined model) had a good performance and applicability. The AUC was 0.968 (95% CI = 0.944–0.986) in the training cohort and 0.873 (95% CI = 0.796–0.940) in the validation cohort. Fig. 3 presents the AUC curves and DCA of the three models in the training and validation cohorts. Fig. 3A and C shows the ROC curves and DCA curves of the three models in the training cohort. Fig. 3B and D shows the ROC curves and DCA curves of the three models in the validation cohort. DCA proved that the combined model had a good clinical application performance.

4.3. Nomogram

R software (version 4.1.2) was used to construct the clinical radiomics nomogram by combining the two independent predictors of clinical factors (PCEA1 and SLDHPADA) and the constructed radiomics score in the training cohort (Fig. 4A) and validation cohort (Fig. 4C). The nomogram included three variables, PCEA1, SLDHPADA and radiomics score. The line segment corresponding to each variable was marked with scales, representing the range of values of the variable, and the length of the line segment reflected the contribution of the factor. The score in the figure represents the corresponding single item score of each variable at different values, and the total score represents the total score of the corresponding single item score after the values of all variables are added up. The bottom is the predicted probability. The closer the predicted calibration curve is to the standard curve, the better the predictive power of the nomogram is. Fig. 4B and D shows the calibration curve. In the training cohort (Fig. 4B), the VIFs of the three variables in the model were 1.297, 1.401 and 1.480, respectively, and there was no multicollinearity. The *C*-index of the model was 0.947 (0.915–0.978), indicating high accuracy. The results of the fit test showed $p > 0.05$, indicating that there was no significant difference between the predicted and observed values, so the model fit was good. In the validation cohort (Fig. 4D), the VIFs of the three variables were 1.029, 1.044 and 1.016, respectively, and it was considered that there was no multicollinearity in the three variables. The *C*-index of the model was 0.831 (0.730–0.933), with moderate accuracy. The model fitted well, with $p > 0.05$ of the goodness-of-fit test.

5. Discussion

In this study, we developed and validated a combined model with better predictive performance in distinguishing MPE from NMPE than those of clinical and radiomics models. The results of this study support the potential clinical application of the nomogram constructed by combining independent clinical predictors and radiomics scores in the diagnosis of MPE in patients using chest CT.

MPE is a common manifestation of pleural involvement in a variety of cancers, such as lung and breast cancers, typically indicating that the tumor has metastasized or progressed to an advanced stage [25–27]. Once patients with cancer develop MPE, their quality of life affected, and their survival time is shortened. Studies have shown that the median survival of patients with MPE varies from 3 to 12 months [28]. Patients with NMPE, such as parapneumonic effusion and tuberculous pleural effusion [29], can usually be cured clinically with timely treatment [30]. Therefore, early and accurate differentiation of MPE and NMPE is important for the development of clinical diagnosis and treatment plans for MPE and for improving patient prognosis.

Researchers have been trying to create effective methods to distinguish MPE from NMPE, but there has been no perfect method. For example, the scoring system constructed by Wang et al. did not incorporate the variable of time of diagnosis into the logistic regression, and the broad applicability is limited because the detection of fluid/serum levels of CEA is not routine around the world [31]. Other researchers have combined the Raman bands of PE with orthogonal partial least squares discriminant analysis to distinguish between

Table 3
Performance of the clinical model, radiomics model, and combined model in the training cohort and validation cohort.

Different Models	Training Cohort (n = 167)				Test Cohort (n = 72)			
	AUC (95% CI)	SEN	SPE	ACC	AUC (95% CI)	SEN	SPE	ACC
Clinical model	0.874 (0.828, 0.916)	0.608	0.954	0.743	0.764 (0.660, 0.857)	0.432	0.857	0.597
Radiomics model	0.878 (0.833, 0.918)	0.873	0.677	0.796	0.808 (0.713, 0.894)	0.864	0.500	0.722
Combined model	0.968 (0.944, 0.986)	0.912	0.923	0.916	0.873 (0.796, 0.940)	0.818	0.857	0.833

Abbreviations: AUC, area under the curve; SEN, sensitivity; SPE, specificity; ACC, accuracy; 95% CI, 95% confidence.

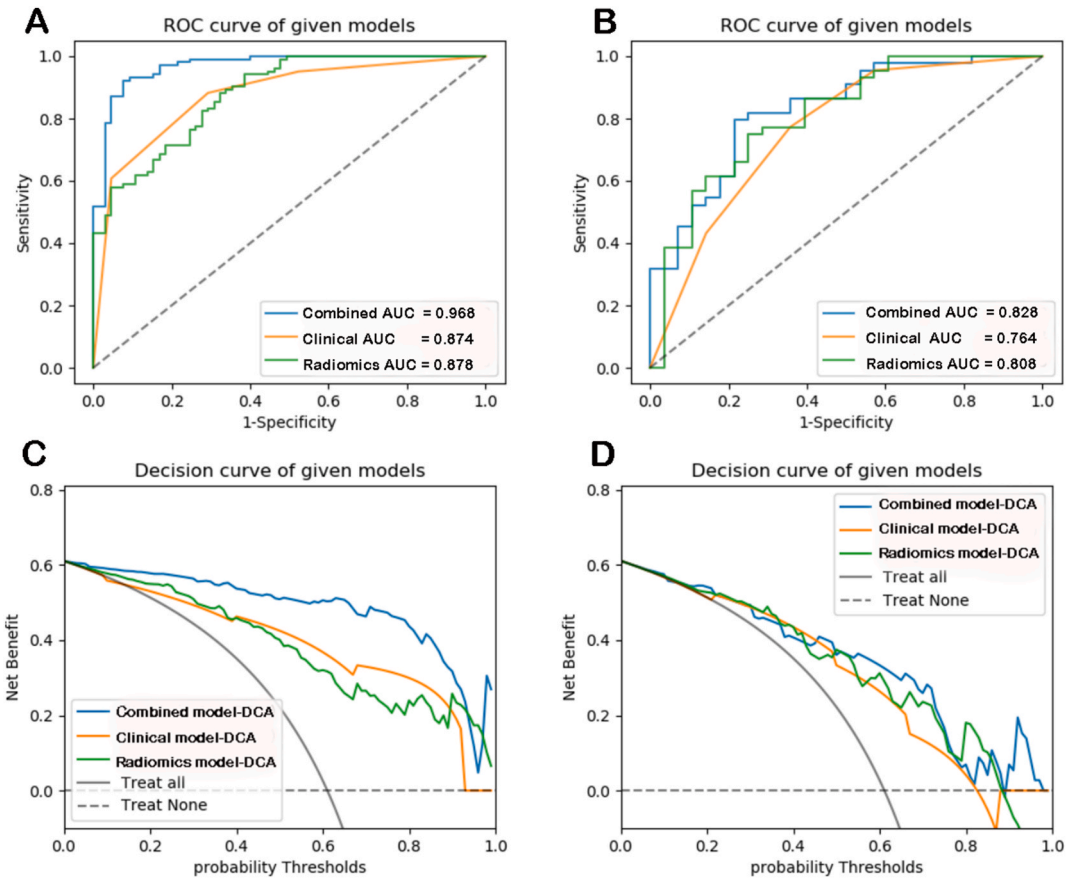

Fig. 3. ROC curves and the decision curve analysis of the three models (A) ROC curves of the three models in the training cohort. (B) ROC curves of the three models in the validation cohort. (C) DCA curves of the three models in the training cohort. (D) DCA curves of the three models in the validation cohort.

MPE and NMPE [32]. The sensitivity and specificity were 92.2% and 93.8%, respectively. In addition, some researchers have established a scoring system for the differential diagnosis of MPE and BPE based on five PET-CT parameters [33]. Due to the high cost and strict requirements for medical equipment, the above methods cannot be promoted and applied in most primary hospitals. Therefore, it is important to design an inexpensive method that can accurately distinguish between MPE and NMPE.

The role of biomarkers in the diagnosis of MPE has been extensively studied [34]. However, which biomarkers should be considered for MPE diagnosis remain controversial. Traditional biomarkers include CEA, CA125, CA19-9, CA15-3, CYFRA 21–1, and NSE; however, their sensitivity and/or specificity are low, and their value in definitive diagnosis is limited [35]. In the construction of this study's clinical model, we selected PCEA1 and SLDHPADA as independent predictors through univariate and multivariate analyses. This finding is consistent with the conclusions of several previous studies. For example, Wang et al. [31] constructed a scoring system to distinguish between MPE and NMPE through multiple regression analysis and found that effusion/serum CEA had high diagnostic significance in the differentiation of MPE and NMPE, with an AUC value of 0.787. Additionally, Hackner et al. found that pleural effusion/serum CEA was a useful predictor of MPE, with a sensitivity of 85% and a specificity of 92% [36]. Concerning SLDHPADA, Verma et al. concluded in a retrospective analysis that the cut-off value of serum LDH:pleural ADA >20 was highly predictive of malignancy in patients with exudative pleural effusion, with high sensitivity and specificity [37].

In this study, in addition to selecting clinical biomarkers, we combined them with radiomics features. By integrating 2 clinical features and 19 imaging features, we constructed a new nomogram model to predict MPE and NMPE. In this study, 19 radiomics features that differed between MPE and NMPE were selected, and these features could not be captured by the naked eye. Quantitative image features based on intensity, shape, size, volume, and texture can provide information about the tumor phenotype and microenvironment that can be correlated with clinical outcome data and used in evidence-based clinical decision support systems [15]. Among the currently available prediction methods, nomograms based on multiple markers have both high accuracy and good discrimination in diagnostic performance, which is convenient for clinical applications [38].

In the training cohort, our study demonstrated that the combined model was superior to both clinical and radiomics models. This implies that incorporating clinical factors into the radiomics model can improve the predictive performance for MPE and NMPE. The sensitivity and accuracy of the combined model were 0.912 and 0.916, respectively, which were higher than those of the clinical and

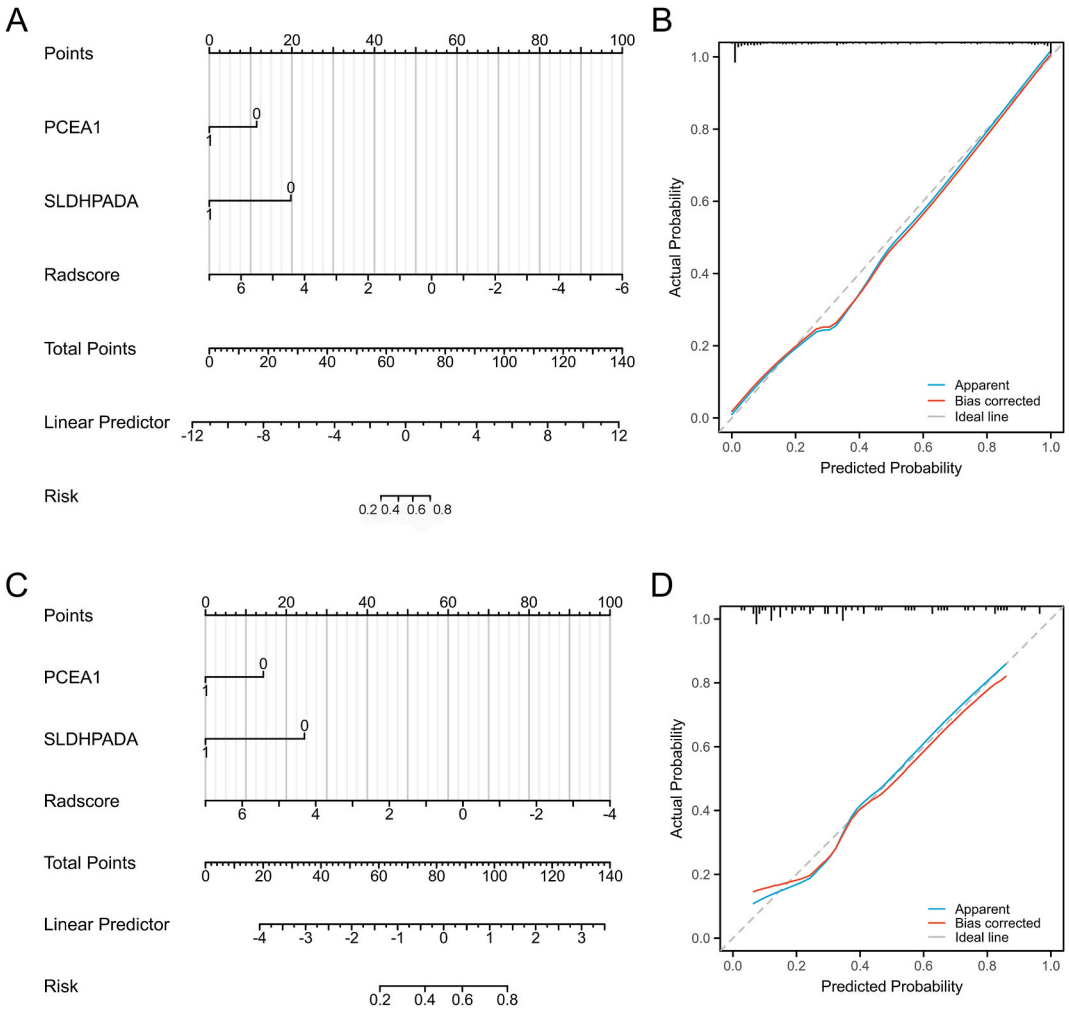

Fig. 4. Nomogram and calibration curve. Clinical radiomics nomogram based on radiomic signatures and clinical factors in the training cohort (A) and validation cohort (C). Calibration curve in the training cohort (B) and validation cohort (D).

radiomics models. However, the specificity of the combined model was lower than that of the clinical model and higher than that of the radiomics model. In the validation cohort, the specificity of the combined model was equal to that of the clinical model and higher than that of the radiomics model. Taken together, the combined model demonstrated better discriminative power than the clinical and radiomics models. DCA showed that the combined model had more net benefits than radiomics and clinical models. Therefore, the nomogram constructed one the basis of both clinical and imaging features can help clinicians distinguish between MPE and NMPE to a certain extent and make effective clinical decisions.

Our study had three major limitations. First, this was a retrospective study, and our findings need to be validated in future prospective studies. Second, our study suggests that effusion/serum CEA and serum LDH/effusion ADA can be used to predict MPE; however, owing to the heterogeneity of detection methods, the best cut-off value is not recommended. Finally, to solve the problem of model overfitting, we used five-fold cross validation in the process of training the model, but the sample size was limited because our sample was from a single medical center. Therefore, further validation with a larger number of patients is needed.

6. Conclusions

CT-based radiomics showed better diagnostic accuracy and model fit than clinical and radiological features for distinguishing MPE from NMPE. The combination of both achieved better diagnostic performance. These findings support the potential clinical application of the nomogram in the diagnosis of patients with MPE using chest CT.

Consent for publication

All authors have reviewed the final version of the manuscript and approved it for publication.

Availability of data and materials

Because the information comes from the hospital case system, the data sets generated and analyzed during the current study period are not publicly available, but can be obtained from the corresponding authors on reasonable request.

Authors' contributions

R Han: conceived and designed the experiments; analyzed and interpreted the data; wrote the paper.
L Huang: performed the experiments.
S Zhou: analyzed and interpreted the data.
J Shen: conceived and designed the experiments.
P Li: conceived and designed the experiments.
M Li: analyzed and interpreted the data.
X Wu: contributed reagents, materials, analysis tools or data.
R Wang: conceived and designed the experiments, wrote the paper.

Funding

This research was supported by the fund for Natural Science Foundation of China (No.81970051), Excellent Top Talent Cultivation Project of Anhui Higher Education Institutions (gxgwfx2021014), A sub-project of the Anhui Medical University National first-class undergraduate specialty construction program (clinical medicine), Construction projects of key disciplines in Hefei (Occupational medicine), the Applied Medical Research Project of Hefei Health Commission (Hwk2021zd008, Hwk2022zd013) and Postgraduate Innovation Research and Practice Program of Anhui Medical University(YJS20230097).

Ethics approval and consent to participate

This retrospective study was approved by the Research Ethics Committee of the First Affiliated Hospital of the Anhui Medical University (Quick-PJ 2022-13-20).

Declaration of competing interest

The authors declare that they have no known competing financial interests or personal relationships that could have appeared to influence the work reported in this paper.

Acknowledgements

Not applicable.

References

[1] R. Bhatnagar, N. Maskell, The modern diagnosis and management of pleural effusions, BMJ (2015) h4520, https://doi.org/10.1136/bmj.h4520.
[2] D. Feller-Kopman, R. Light, Pleural Disease, N. Engl. J. Med. 8 (2018) 740–751, https://doi.org/10.1056/NEJMra1403503.
[3] F.K. Paddock, The diagnostic significance of serous fluids in disease, N. Engl. J. Med. 25 (1940) 1010–1015, https://doi.org/10.1056/NEJM194012192232503.
[4] R.W. Light, M.I. Macgregor, P.C. Luchsinger, W.C. Ball Jr., Pleural effusions: the diagnostic separation of transudates and exudates, Ann. Intern. Med. 4 (1972) 507–513, https://doi.org/10.7326/0003-4819-77-4-507.
[5] J.E. Heffner, L.K. Brown, C.A. Barbieri, Diagnostic value of tests that discriminate between exudative and transudative pleural effusions. Primary Study Investigators, Chest 4 (1997) 970–980, https://doi.org/10.1378/chest.111.4.970.
[6] M.E. Wilcox, C.A. Chong, M.B. Stanbrook, et al., Does this patient have an exudative pleural effusion? The Rational Clinical Examination systematic review, JAMA 23 (2014) 2422–2431, https://doi.org/10.1001/jama.2014.5552.
[7] G.F. Tassi, G. Cardillo, G.P. Marchetti, F. Carleo, M. Martelli, Diagnostic and therapeutical management of malignant pleural effusion, Ann. Oncol. (2006) ii11–12, https://doi.org/10.1093/annonc/mdj911.
[8] D.J. Feller-Kopman, C.B. Reddy, M.M. DeCamp, et al., Management of malignant pleural effusions. An official ATS/STS/STR clinical practice guideline, Am. J. Respir. Crit. Care Med. 7 (2018) 839–849, https://doi.org/10.1164/rccm.201807-1415ST.
[9] R. Bennett, N. Maskell, Management of malignant pleural effusions, Curr. Opin. Pulm. Med. 4 (2005) 296–300, https://doi.org/10.1097/01.mcp.0000166495.71574.46.
[10] Y. Yang, Y.L. Liu, H.Z. Shi, Diagnostic accuracy of combinations of tumor markers for malignant pleural effusion: an updated meta-analysis, Respiration 1 (2017) 62–69, https://doi.org/10.1159/000468545.
[11] C. Alemán, L. Sanchez, J. Alegre, et al., Differentiating between malignant and idiopathic pleural effusions: the value of diagnostic procedures, QJM 6 (2007) 351–359, https://doi.org/10.1093/qjmed/hcm032.
[12] A.T. Society, Management of malignant pleural effusions, Am. J. Respir. Crit. Care Med. 5 (2000) 1987–2001, https://doi.org/10.1164/ajrccm.162.5.ats8-00.
[13] M. Aboudara, F. Maldonado, Update in the management of pleural effusions, Med. Clin. 3 (2019) 475–485, https://doi.org/10.1016/j.mcna.2018.12.007.
[14] J.M. Porcel, M. Pardina, S. Bielsa, A. González, R.W. Light, Derivation and validation of a CT scan scoring system for discriminating malignant from benign pleural effusions, Chest 2 (2015) 513–519, https://doi.org/10.1378/chest.14-0013.
[15] R.J. Gillies, P.E. Kinahan, H. Hricak, Radiomics: images are more than pictures, they are data, Radiology 2 (2016) 563–577, https://doi.org/10.1148/radiol.2015151169.
[16] P. Lambin, R.T.H. Leijenaar, T.M. Deist, et al., Radiomics: the bridge between medical imaging and personalized medicine, Nat. Rev. Clin. Oncol. 12 (2017) 749–762, https://doi.org/10.1038/nrclinonc.2017.141.

[17] R. Sun, E.J. Limkin, M. Vakalopoulou, et al., A radiomics approach to assess tumour-infiltrating CD8 cells and response to anti-PD-1 or anti-PD-L1 immunotherapy: an imaging biomarker, retrospective multicohort study, Lancet Oncol. 9 (2018) 1180–1191, https://doi.org/10.1016/s1470-2045(18)30413-3.
[18] J. Gong, X. Bao, T. Wang, et al., A short-term follow-up CT based radiomics approach to predict response to immunotherapy in advanced non-small-cell lung cancer, #N/A 1 (2022), 2028962, https://doi.org/10.1080/2162402x.2022.2028962.
[19] Y.Q. Huang, C.H. Liang, L. He, et al., Development and validation of a radiomics nomogram for preoperative prediction of lymph node metastasis in colorectal cancer, J. Clin. Oncol. 18 (2016) 2157–2164, https://doi.org/10.1200/jco.2015.65.9128.
[20] P.A. Yushkevich, J. Piven, H.C. Hazlett, et al., User-guided 3D active contour segmentation of anatomical structures: significantly improved efficiency and reliability, Neuroimage 3 (2006) 1116–1128, https://doi.org/10.1016/j.neuroimage.2006.01.015.
[21] T.K. Koo, M.Y. Li, A guideline of selecting and reporting intraclass correlation coefficients for reliability research, J Chiropr Med 2 (2016) 155–163, https://doi.org/10.1016/j.jcm.2016.02.012.
[22] van Griethuysen Jjm, A. Fedorov, C. Parmar, et al., Computational radiomics system to decode the radiographic phenotype, Cancer Res. 21 (2017) e104–e107, https://doi.org/10.1158/0008-5472.Can-17-0339.
[23] A. Zwanenburg, S. Leger, Martin Vallières, S. Löck, Image biomarker standardisation initiative, Radiology 21 (2016).
[24] J.A. Hanley, B.J. McNeil, The meaning and use of the area under a receiver operating characteristic (ROC) curve, Radiology 1 (1982) 29–36, https://doi.org/10.1148/radiology.143.1.7063747.
[25] A.C. Bibby, P. Dorn, I. Psallidas, et al., ERS/EACTS statement on the management of malignant pleural effusions, Eur. Respir. J. 1 (2018), https://doi.org/10.1183/13993003.00349-2018.
[26] M. Guo, F. Wu, G. Hu, et al., Autologous tumor cell-derived microparticle-based targeted chemotherapy in lung cancer patients with malignant pleural effusion, Sci. Transl. Med. 474 (2019), https://doi.org/10.1126/scitranslmed.aat5690.
[27] S. Muruganandan, M. Azzopardi, D.B. Fitzgerald, et al., Aggressive versus symptom-guided drainage of malignant pleural effusion via indwelling pleural catheters (AMPLE-2): an open-label randomised trial, Lancet Respir. Med. 9 (2018) 671–680, https://doi.org/10.1016/s2213-2600(18)30288-1.
[28] M.E. Roberts, E. Neville, R.G. Berrisford, G. Antunes, N.J. Ali, Management of a malignant pleural effusion: British thoracic society pleural disease guideline 2010, Thorax (2010) 32–40, https://doi.org/10.1136/thx.2010.136994.
[29] H. Hamm, R.W. Light, Parapneumonic effusion and empyema, Eur. Respir. J. 5 (1997) 1150–1156, https://doi.org/10.1183/09031936.97.10051150.
[30] E.O. Bedawi, J. Guinde, N.M. Rahman, P. Astoul, Advances in pleural infection and malignancy, Eur. Respir. Rev. 159 (2021), https://doi.org/10.1183/16000617.0002-2020.
[31] S. Wang, S. Tian, Y. Li, et al., Development and Validation of a Novel Scoring System Developed from a Nomogram to Identify Malignant Pleural Effusion, #N/A, 2020, 102924, https://doi.org/10.1016/j.ebiom.2020.102924.
[32] K. Liu, S. Jin, Z. Song, L. Jiang, High accuracy detection of malignant pleural effusion based on label-free surface-enhanced Raman spectroscopy and multivariate statistical analysis, Spectrochim. Acta Mol. Biomol. Spectrosc. (2020), 117632, https://doi.org/10.1016/j.saa.2019.117632.
[33] M.F. Yang, Z.H. Tong, Z. Wang, et al., Development and validation of the PET-CT score for diagnosis of malignant pleural effusion, Eur. J. Nucl. Med. Mol. Imag. 7 (2019) 1457–1467, https://doi.org/10.1007/s00259-019-04287-7.
[34] M. Zhang, L. Yan, G. Lippi, Z.D. Hu, Pleural biomarkers in diagnostics of malignant pleural effusion: a narrative review, Transl. Lung Cancer Res. 3 (2021) 1557–1570, https://doi.org/10.21037/tlcr-20-1111.
[35] C. Cheng, Y. Yang, W. Yang, D. Wang, C. Yao, The diagnostic value of CEA for lung cancer-related malignant pleural effusion in China: a meta-analysis, Expet Rev. Respir. Med. 1 (2022) 99–108, https://doi.org/10.1080/17476348.2021.1941885.
[36] K. Hackner, P. Errhalt, S. Handzhiev, Ratio of carcinoembryonic antigen in pleural fluid and serum for the diagnosis of malignant pleural effusion, Ther. Adv. Med. Oncol. 1758835919850341 (2019), https://doi.org/10.1177/1758835919850341.
[37] A. Verma, J. Abisheganaden, R.W. Light, Identifying malignant pleural effusion by A cancer ratio (serum LDH: pleural fluid ADA ratio), Lung 1 (2016) 147–153, https://doi.org/10.1007/s00408-015-9831-6.
[38] S.F. Shariat, U. Capitanio, C. Jeldres, P.I. Karakiewicz, Can nomograms be superior to other prediction tools? BJU Int. 4 (2009) 492–495, https://doi.org/10.1111/j.1464-410X.2008.08073.x, discussion 495-497).